China Ocean Eng., 2020, Vol. 34, No. 3, P. 299–313
DOI: https://doi.org/10.1007/s13344-020-0028-2, ISSN 0890-5487
http://www.chinaoceanengin.cn/ E-mail: coe@nhri.cn

# Weather Induced Quasi-Periodic Motions in Estuaries and Bays: Meteorological Tide

LI Chun-yan<sup>a,\*</sup>, HUANG Wei<sup>a,b</sup>, WU Ren-hao<sup>c,d,\*</sup>, Alex SHEREMET<sup>e</sup>

- <sup>a</sup> College of the Coast and Environment, Louisiana State University, Baton Rouge 70803, USA
- <sup>b</sup> Virginia Institute of Marine Science, College of William and Mary, Gloucester Pt. 23062, USA
- <sup>c</sup> School of Atmospheric Sciences, Sun Yat-Sen University, Zhuhai 519082, China
- <sup>d</sup> Southern Marine Science and Engineering Guangdong Laboratory (Zhuhai), Zhuhai 519082, China
- <sup>e</sup> Engineering School of Sustainable Infrastructure and Environment, University of Florida, Gainesville FL 32611, USA

Received January 14, 2020; revised February 25, 2020; accepted March 12, 2020

©2020 Chinese Ocean Engineering Society and Springer-Verlag GmbH Germany, part of Springer Nature

#### Abstract

Influenced by weather, the estuaries and bays often exhibit recurring oscillations in flow and water level similar to astronomical tides. The weather impact however is less regular than tides and more difficult to predict. The spectrum of weather induced motions in estuaries and bays is mostly at the low-frequency end with time scales longer than those of diurnal tides. The repeated weather impact produces meteorological tide: the recurring flood and ebb and flushing of the estuaries and bays but at lower frequencies than those of tides. The variation in weather conditions is quasi-periodic and of large scale nature (~1000-3000 km) because of the alternating low- and high- atmospheric pressure systems of extra-tropical cyclones and anti-cyclones and associated fronts. By examining 40 years of data between Jan. 1, 1977 and Dec. 31, 2016, we identified 1648 frontal events (averaging ~41.2±4.7 per year) influencing the northern Gulf of Mexico for time periods in the spring, fall and winter. The late spring and summer months (May, Jun, July, and August) were not included in the calculation because of much weaker activities involving synoptic weather systems with fronts during these months. It is found that the number of frontal events reached the maximum in Jan. and Dec. while the minimum occurred in April and Sept. It is found that there is an increasing trend of number of fronts over the 40-year period. Our data show that the low pass filtered water level, velocity, and vorticity (velocity shear) all vary in response to the weather and appear as the meteorological tide. The particle excursions of meteorological tides are much larger than those from the astronomical tides. In addition, the irregular nature of the meteorological tide makes the inward flux and outward flux asymmetric in general and thus it has a significant implication to dispersion and transport of waterborne materials. A scaling analysis shows that the meteorological tide generally reaches quasi-steady state; and as a result, a regression model is established which can be very useful for predicting the weather produced quasi-periodic motions.

**Key words:** meteorological tide, atmospheric fronts, particle excursion, quasi-steady state, northern Gulf of Mexico, estuarine exchange flows

Citation: Li, C. Y., Huang, W., Wu, R. H., Sheremet, A., 2020. Weather induced quasi-periodic motions in estuaries and bays: meteorological tide. China Ocean Eng., 34(3): 299–313, doi: https://doi.org/10.1007/s13344-020-0028-2

## 1 Introduction

Estuarine circulations can be generated by many mechanisms. The first of which being studied is the gravitational circulation (Pritchard, 1952, 1954, 1956; Hansen and Rattray, 1965; Aubrey and Friedrichs, 1996; Valle-Levinson, 2010; de Miranda et al., 2017). As a result, a vorticity is generated by gravity and a horizontal density gradient so that the fresher water tends to flow on the surface toward the ocean and the saltier ocean water tends to flow land-

ward in the lower layer with turbulent mixing in between (Fig. 1).

Another mechanism which has been extensively studied is the tidally-induced flows (Charlton et al., 1975; Friedrichs and Aubrey, 1994; Robinson, 1960; Ianniello, 1977, 1979). Astronomical tide in the ocean is produced in the deep ocean by tide-generating force of the Moon and Sun and propagated into shallow waters. Tidal currents are periodic with known discrete frequencies and thus re-

Foundation item: The research was financially supported by the National Science Foundation and Natural Environment Research Council (Grant Nos. NSF-NERC 1736713 and NSF-NERC 1737274), Bureau of Ocean Energy Management (Grant No. M15AC000015), NOAA-NOS-IOOS-2016-2004378, through the Northern Gulf Institute by NOAA's Office of Ocean and Atmospheric Research.

<sup>\*</sup>Corresponding authors. E-mail: cli@lsu.edu; wurenhao@mail.sysu.edu.cn

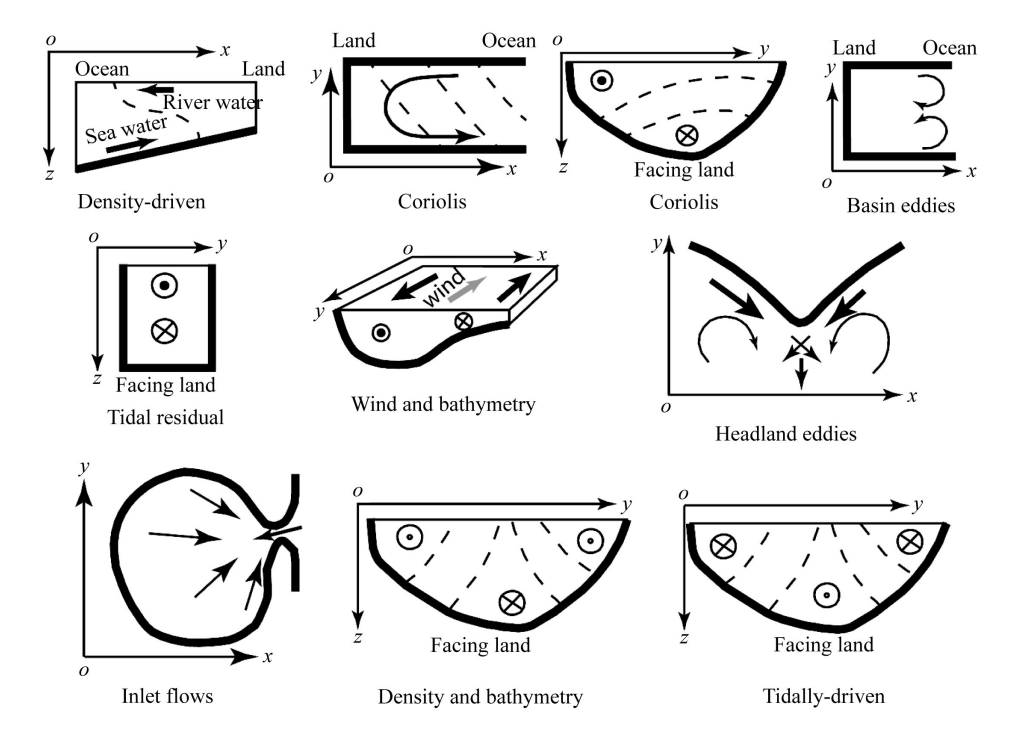


Fig. 1. Various estuarine circulation modes. These include density-driven (gravitational) circulation, estuarine circulation under Coriolis effect (horizontal view), estuarine exchange flow with Coriolis effect (vertical view), basin eddies, tidal residuals (vertical view), wind-driven flow with cross channel depth variation, headland eddies, inlets flows, density-driven flow with depth variation, and tidally-driven flows with depth variation, respectively.

peatedly flow into and out of estuaries and bays (Officer, 1976; Prandle, 2009). The flood and ebb currents however roughly cancel each other to yield an almost zero net flow at the first order of approximation, correct to a/h, in which a and h are the tidal amplitude and mean water depth, respectively. A net flow (Fig. 1) can be generated at the second order ( $\sim (a/h)^2$ ) by nonlinearity, which includes the combined effects of finite amplitude of tidal wave, advection, and the bottom friction (Li et al., 1998; Li and O'Donnell, 1997, 2005).

Both the net flows by gravitational circulation and nonlinear tide are affected by bathymetry or water depth variations in the estuaries and bays (Fig. 1). For example, a lateral depth variation in an estuarine channel would make the two-layered gravitational circulation "tilted" sideway so that the shallow water tends to have outward flow and the deeper water inward flows (Wong, 1994). The tidally induced flows also have lateral structures or shears if the depth varies across the channel (Li and O'Donnell, 1997). The actual net flow distribution is a little complicated as it depends on the dynamic length of the estuary (a ratio between the channel length and the tidal wavelength so that the net flows in short and long channels are different (Li and O'Donnell, 2005). There are also the effects (Fig. 1) of Earth's rotation (Pritchard, 1952; Doyle and Wilson, 1978; Kasai et al., 2000; Valle-Levinson et al., 2003), constriction of an inlet (Stommel and Farmer, 1952; Fischer et al., 1979), channel curvature (Li et al., 2008), and headland (Pingree and Maddock, 1977a, 1977b, 1979; Pingree, 1978; Maddock and

Pingree, 1978; Fang and Yang, 1985; Signell and Geyer, 1991; Geyer, 1993; Wolanski et al., 1996; Chant and Wilson, 1997).

In addition to the above mechanisms, wind also contributes to the estuarine circulations (Chuang and Swenson, 1981; Kjerfve, 1973; Herrling and Winter, 2015; Sanay and Valle-Levinson, 2005; Schoen et al., 2014). This was recognized even in the early days of the study on gravitational circulations (Barlow, 1956). The effect of wind however was not widely appreciated for quite some time. A study (Elliot, 1978) based on the Empirical Orthogonal Function (EOF) analysis on observational data reveal that a few modes of exchange flows can be generated by wind: flows can be all-in, all-out, top-in and bottom-out or top-out and bottom-in, or having even more complicated three-layer structures, etc.

Estuaries and bays may have more than one opening to the coastal ocean. The wind-driven exchange flows in a multiple inlet system are found to be much more significant than tidally induced flows (Li, 2013). This is mainly because with multiple inlets, through-flows (Fig. 2) can be generated easily by winds one way or the other so that some inlet(s) may have inward flows while the other inlet(s) may have outward flows (Li, 2013; Li et al., 2019a). The pattern can of course change with the change of wind as demonstrated in Li et al. (2019a).

The winds that drive circulations in estuaries and bays are not random forcing. The variations in wind are oftentimes part of largescale atmospheric circulations. By larges-

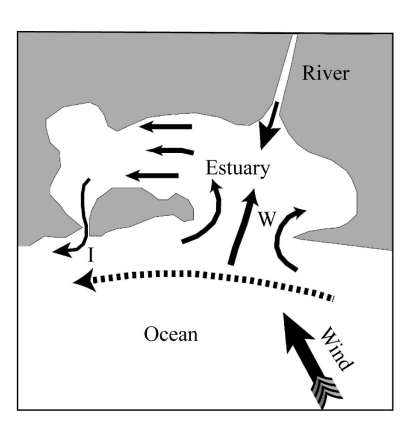


**Fig. 2.** Schematic diagram of wind-driven estuarine through flow if there are more than one inlet. With a given wind condition, one inlet may have a predominantly inward flow, while another inlet may have an outward flow.

cale, we mean a spatial scale of ~1000 km or larger. Wind events at sea level are often experienced as part of a synoptic weather system (Fig. 3) that is developed along the westerly wind systems of the atmosphere in the upper troposphere (Holton and Hakim, 2012). Of course, an exception is the system developed in the tropics - the tropical cyclones (e.g. typhoons for the Pacific region and hurricanes for the Atlantic region). However, tropical cyclones usually do not impact the same location regularly. The associated damages due to them are case dependent, and many studies have been done on the impact of hurricanes to the coast. In contrast, the atmospheric frontal events under the largescale atmospheric circulations are much more frequent, occurring every 3-10 days, particularly from Fallto Spring (Roberts et al., 1987, 1989, 2015; Moeller et al., 1993; Li and Chen, 2014). They have cumulative effects in driving the hydrodynamics and affecting the geomorphology (Keen and Stavn, 2012; Kineke et al., 2006; Chuang and Wiseman,

## 1983; Siadatmousavi and Jose, 2015).

In short, there is an entire category of synoptic-scale weather systems including extratropical systems associated with centers of low- (cyclones) and high- (anticyclones) pressures. A sea-level air pressure trough can form between high pressure systems as the boundary (or front) of different air masses. The front can be extended from the center of a low air pressure system along a trough of thousands of km. Fronts are usually lines with strong wind shears and sharp gradients of temperature and humidity. The spatial scales of these atmospheric fronts are much larger than those of coastal ocean and estuarine problems: the fronts typically stretch 2000–3000 km (Li et al., 2018, 2019a, 2019b). As a result, the impact of these frequent atmospheric fronts can be over a much larger area than the area of major influence of a tropical cyclone. In the northern Gulf of Mexico, every year there are 30–50 frontal systems passing the area; most of them are cold fronts (Fig. 3), some are warm fronts and stationary fronts. Stationary fronts are either a cold or warm front in pause or a precursor of a cold or warm front, depending on which direction it would start to move to. Both cold and warm fronts can produce significant perturbations to the coastal waters as demonstrated in Li et al. (2018). The strong wind forces the water to oscillate, driving the water and sediment exchanges with the coastal ocean (Li et al., 2017).

Because of the repeated actions of these synoptic weather systems over a large scale in the coastal region, the resultant exchange flows in estuaries are "tide-like" in the sense that they are quasi-periodic, even though we must recognize that their regularity is much less obvious when compared to that of tide. This can be seen from the continuous nature of the spectra for weather induced motion particu-

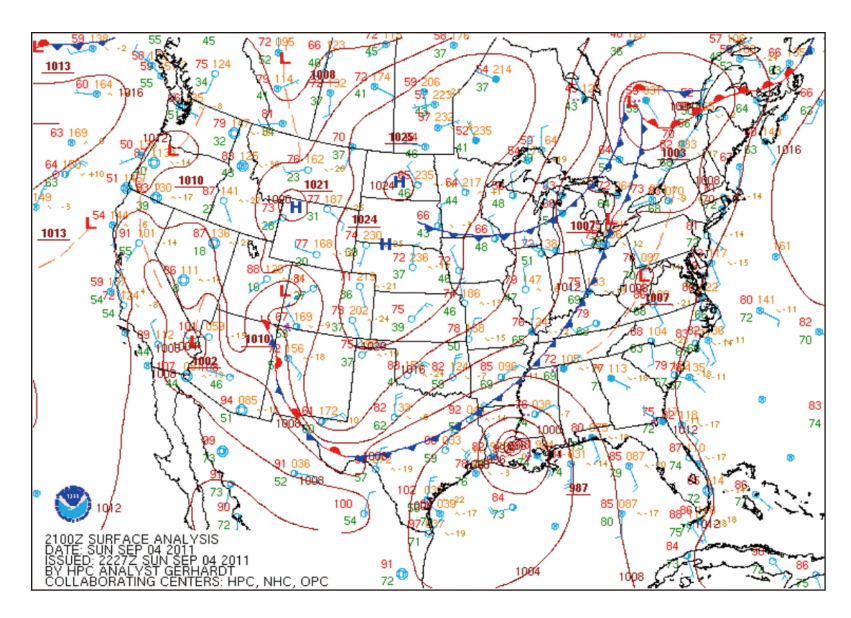


Fig. 3. A weather map from NOAA showing atmospheric cold, warm, and stationary fronts, and a tropical storm on 21:00 UTC, Sep. 4, 2011 (Tropical Storm Lee located at central northern Gulf of Mexico).

larly between 0.1 and 0.3 cycle per day in frequency (or ~ 3–10 days in period). In a study on the exchange flows driven by repeated cold fronts in three bays in the coastal Louisiana (Feng and Li, 2010), it is demonstrated that a single cold front event can drive 40% of the bay water onto the shelf in 30–40 hours. Li et al. (2018) examined the estuarine exchange flows at Port Fourchon by 76 atmospheric frontal processes including cold, warm, and combinations of cold-warm fronts. Li et al. (2019a) also studied the impact of 51 atmospheric front induced exchange flows through the multiple inlet system of Barataria Bay using data from multiple ADCPs.

Because of the quasi-periodic nature, the weather induced dynamical processes are called meteorological tide. We will present a preliminary analysis of a 40-year dataset of the cold front events in the northern Gulf of Mexico for atmospheric frontal events, followed by some case studies of meteorological tides using oceanographic data at an inlet of a bay, including an analysis of vorticity in response to the meteorological forcing.

## 2 Atmospheric fronts and meteorological tide

Atmospheric frontal events repeat themselves every few days across a large area of several thousand kilometers. The large influencing area and repeatability make the estuarine response quasi-periodic and thus the term meteorological tide is used for this type of motions. In Feng and Li (2010), 29 cold fronts were identified for an 8-month period in late 2006 and early 2007. The subtidal response of water level to the atmospheric events was obvious from the low pass filtered data. In Li et al. (2018), a total of 76 atmospheric fronts were identified for a period of 515 days when an AD-CP was deployed at a tidal channel at Port Fourchon of Louisiana. These atmospheric fronts include both cold and warm fronts, as well as combinations of them, e.g. double cold fronts, cold-warm-cold fronts, and warm-cold fronts. The low pass filtered water velocity as well as the low pass filtered total along-channel transport across the channel was shown to be aligned in time with the frontal passage: each event corresponded to a spike in the total transport.

In Weeks et al. (2018), a time series of 717 days of AD-CP data was used to analyze the effect of cold fronts to the subtidal volume transport of Vermillion Bay through its southwest inlet and the largest event for this time period was discussed. By examining NOAA's water level data from a nearby station, a total of 46 significant water level variation events were identified for a period of about 10 years, which were all associated with extreme weather (major cold fronts and one tropical cyclone).

In another study for the exchange flows through the three-inlet Lake Pontchartrain (Huang and Li, 2017), 5 cold front induced net flows were examined and it was found with a numerical model experiment that the overall water level was determined by the so-called remote wind effect

while the water slope inside the estuary was determined by the local wind stress.

In a study for the exchange flows through the multi-inlet Barataria Bay using several long-term horizontal AD-CPs, it was found that the exchange flows respond significantly to 51 atmospheric cold fronts with three empirical modes associated with different wind effects (Li et al., 2019a). These modes include the all-in and all-out flows modes and also different kinds of throughflow patterns with some inlet(s) having inward flows while the other inlet(s) having outward flows as discussed in Li (2013): e.g. shallow inlets tend to have downwind flows while deeper inlets upwind flows; upwind inlets tend to have inward flows and downwind inlets outward flows if wind is along the shore but slightly onshore or offshore, given that these inlets are all along the same coastline. In Wang et al. (2020), winddriven exchange flows through a narrow dredged channel of Calcasieu Lake Estuary were studied and a regression model proposed in Li et al. (2019a, 2019b) was applied for 12 years of data and identified 212 wind-driven outward flux events.

With these studies, here we extend the time period to examine the variations in the atmospheric frontal events. More specifically, here we examine weather data for the entire contiguous U.S. from NOAA for a period between Jan. 1, 1977 to Dec. 31, 2016, a total of 40 years. Since the summertime is a period with very little synoptic scale atmospheric motion except occasional tropical cyclones, we exclude the time from May 1 to August 31, i.e., for each year, we counted the frontal events from Jan. 1 to April 30 and from Sept. 1 to Dec. 31, a total of eight months. All the atmospheric frontal events are identified from weather maps and counted for each month. The results are given in Table 1. These fronts all affected the northern Gulf of Mexico. To be more precise, they all passed the state of Louisiana. It is interesting to note that there seems a tendency of increasing number of total frontal events per year over the 40-year time period (Fig. 4a). A linear regression gives a slope of 0.2039 fronts/year. If we multiple the slope with 40 years, it yields a value of 8.15 fronts. In other words, compared to the year 1977, the year 2016 has 8.15 more frontal events, excluding the random fluctuations (i.e. if we accept the linear model of Fig. 4a). Is this a result of global climate change? It would be a great subject of study. However, this study does not focus on the climate change issue. We will have to defer that study to a subsequent investigation.

The main message is that the numbers of atmospheric frontal events are quite persistent over the years. It is found that in the month of January, there were 252 such events over the 40 years; in February, there were 228 events; in March, 222 events; April, 191; in September, 121; October, 180; November, 222; and December, 232. The average monthly numbers of events are shown in Fig. 4b. More specifically, January, February, March, April, September, Oc-

Table 1 Atmos	Jan.	Feb.	Mar.	Apr.	Sep.	Oct.	Nov.	Dec.	Total
1977	5	5	4	2	2	6	6	6	36
1978	4	3	4	3	1	5	5	6	31
1979	6	4	4	5	3	6	4	4	36
1980	7	6	9	5	2	5	6	7	47
1981	6	5	6	5	4	5	6	9	46
1982	5	6	2	6	4	5	5	6	39
1983	7	4	3	5	2	4	6	5	36
1984	5	5	5	6	3	3	6	4	37
1985	5	4	6	3	4	3	5	4	34
1986	5	6	4	3	2	3	7	4	34
1987	6	5	4	4	3	4	4	5	35
1988	4	5	6	6	3	6	7	6	43
1989	8	4	4	4	3	3	5	7	38
1990	5	5	6	5	2	5	5	6	39
1991	6	5	6	5	2	5	5	6	40
1992	5	4	5	4	3	5	6	7	39
1993	7	4	6	6	7	3	5	7	45
1994	7	4	6	6	4	2	6	3	38
1995	5	7	4	4	5	6	6	4	41
1996	7	5	5	5	4	5	6	6	43
1997	7	4	8	5	3	4	7	4	42
1998	7	5	5	5	2	3	4	6	37
1999	7	7	6	4	4	5	4	7	44
2000	5	7	8	8	3	2	6	8	47
2001	7	6	5	4	3	4	4	6	39
2002	6	7	7	4	4	7	7	5	47
2003	7	6	7	4	3	6	5	8	46
2004	5	5	7	4	4	5	7	5	42
2005	5	4	8	6	2	4	7	8	44
2006	7	8	7	5	5	5	5	5	47
2007	7	8	3	6	2	3	6	8	43
2008	9	8	6	5	3	4	8	7	50
2009	10	8	5	7	3	7	4	8	52
2010	6	6	5	4	2	5	6	5	39
2011	7	6	6	4	4	4	5	5	41
2012	7	5	4	6	3	5	5	6	41
2013	5	10	4	5	2	6	4	4	40
2014	10	7	6	4	2	5	6	6	46
2015	8	7	7	5	3	5	6	4	45
2016	5	8	9	4	1	2	5	5	39
Total	252	228	222	191	121	180	222	232	1648

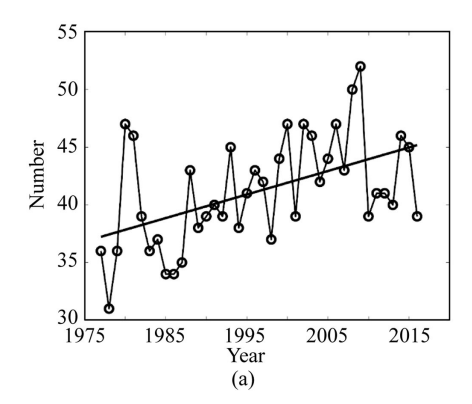
tober, November, and December have monthly average of 6.3, 5.7, 5.55, 4.78, 3.03, 4.5, 5.55, 5.80 events, respectively. Clearly the number of events per month is the maximum in January and December and decreases both directions so that April and September had the lowest numbers. All the frontal events added together to a total of 1648 events. This yields an average of ~ 41.2 events per year for the 8-month period, with a standard deviation of 4.7. Note that most of these atmospheric fronts swept through the entire coastal region of northern Gulf of Mexico and thus had a widespread influence on the coastal ocean dynamics.

It is important to reiterate that these persistent atmospheric events provide the quasi-periodic forcing to drive the coastal ocean and estuarine responses in a quasi-periodic fashion to produce the meteorological tides. In the following, we will discuss a case study using in situ observations of the exchange flows in the Barataria Pass of Barataria Bay.

## 3 Case studies

#### 3.1 Study site and flow velocity data

The recent studies of atmospheric frontal event induced estuarine flows or meteorological tides in estuaries through multiple inlets (Huang and Li, 2017, 2019; Li et al., 2018, 2019a, 2019b) focused on the overall exchanges between the estuaries and coastal ocean. In the following, we exam-



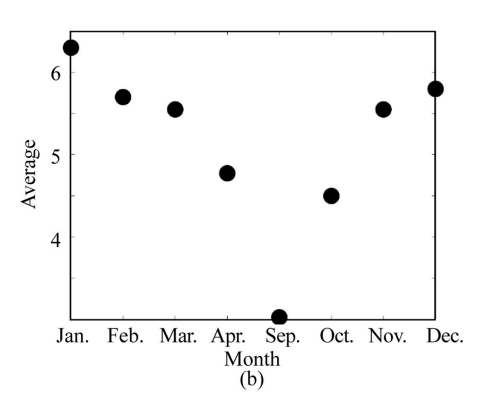


**Fig. 4.** Counts of atmospheric frontal events affecting the Louisiana coast from 1977 to 2016. (a) The total fronts in each year for the eight months: Jan., Feb., Mar., Apr., Sep., Oct., Nov., and Dec., respectively. The solid straight line is a linear regression. (b) The number of fronts in each of the eight months averaged over the 40-year period.

ine the meteorological tides by using high-resolution data that allow us to look into the velocity, velocity shears and relative vorticity, in response to the weather forcing, which are important for estuarine turbulence mixing and dispersion (Fischer et al., 1979).

Barataria Bay (Fig. 5) is an irregularly shaped shallow estuary with a horizontal dimension of roughly 40 km×40 km, with its axis oriented in the northwest-southeast directions (Li et al., 2011a). The bay is located south of the city of New Orleans. It is bounded by the past and present Mississippi River ridges. The bay has several tidal inlets connecting with the coastal ocean of Louisiana Bight. The major inlets include Barataria Pass with a maximum width of 800 m at the mouth. Barataria Pass is one of the main outlets of freshwater from the Barataria Basin because it is the deepest. The main freshwater source of Barataria Bay is the Mississippi River water through the man-made Davis Pond Diversion facility, which has a capacity of about 250 m<sup>3</sup>/s. The bay has an average depth of about 2 m. The main inlet (Barataria Pass) has a depth of slightly larger than 20 m (Li et al., 2011a). Inside the inlet there is a circular shaped depression of close to 50 m deep which is the deepest location

in all the Louisiana lagoons, bays, and estuaries, according to our observations using acoustic transducers (Li et al., 2011ba, 2019a). This suggests a strong current caused erosion. Tide in this region is mainly micro and diurnal with a relatively small maximum amplitude of  $\sim 0.6~\text{m}$  tidal range (Harris, 1981; Forbes, 1988). It is shown in Li et al. (2019a) that the tidal and subtidal spectra have comparable magnitudes (tidal is 22%–29% and subtidal is 23%–31% of the total amplitude spectrum). The subtidal component is mainly wind-driven.

Starting from March 2, 2011, we deployed an acoustic Doppler current profiler (ADCP). It was a Nortek Continental 470 kHz frequency horizontal ADCP, mounted at about 2.2 m below the mean surface. It included a pressure sensor recording the water elevation variations, and two velocity transducers for profiles of the two horizontal velocity components. The instrument was mounted at (29°16′21.37″, 89°56′46.78″) on a treated wooden piling at the eastern side of the inlet. The transducers were mounted looking southwestward to cover a maximum width of 160 m. The data had only a brief gap in time (less than 2 hours) when the first half of data were downloaded in the middle of the de-

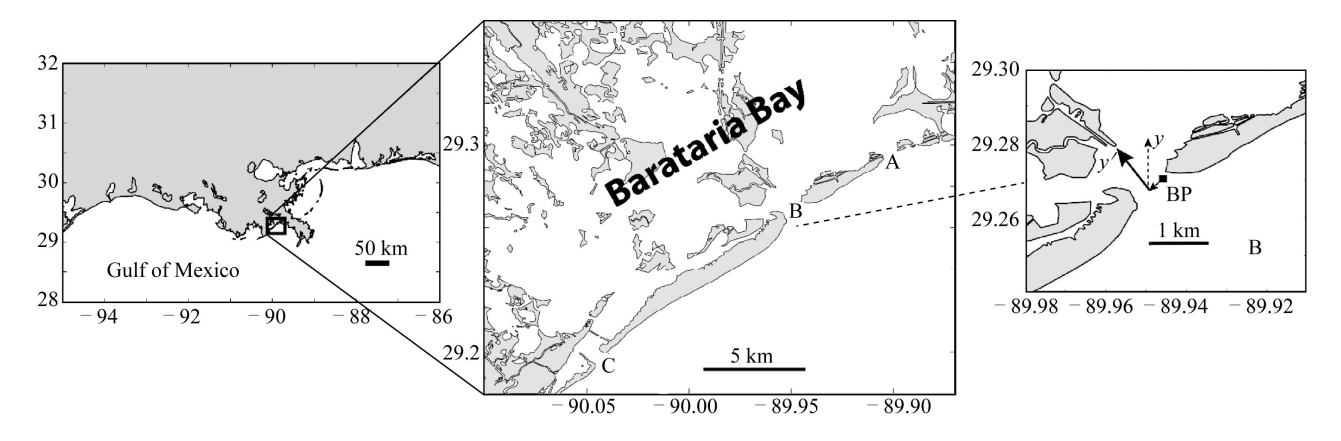


**Fig. 5.** Study site: Barataria Bay, Barataria Pass, and the ADCP location. The inlets marked with A, B, and C are Pass Abel, Barataria Pass, and Caminada Pass, respectively. The ADCP was deployed at the site marked by a solid rectangle. The arrow from the rectangle shows the direction the ADCP beams were facing. The y-axis is toward the north and y'-axis is along the channel toward the inside of the bay.

ployment period. The first data file was between 4:52:00, March 2, 2011 and 17:22:00, July 12, 2011; and the second between 18:59:08, July 12, 2011 and 15:44:08, Sept. 8, 2011. These two files used identical instrument setup. The data have 40 bins of velocity across the channel at 4 m intervals from 5 m to 161 m away from the transducers. Data were recorded at 15-min intervals.

## 3.2 Analysis and results

Other than the single gap of less than 2 hours, the data retrieved were excellent with no gaps for the 15-min interval data. The measured velocity vectors are in the East-North coordinate system. A 52.7° counterclockwise rotation was applied to transform the velocity data to the along channel and cross channel flow components. The analysis was all done to the rotated data.

The along channel velocity time series at a mid-channel position or ~80 m from the ADCP sensors and its low pass filtered variations are shown in Fig. 6a. In comparison, the cross-channel velocity component is much smaller although tidal signal still exists (Fig. 6b). In Li et al. (2011a), velocity profiles across the channel of Barataria Pass were measured by a vessel-based ADCP through a repeated occupa-

tion of a cross-channel transect over ~24 hr. The present data using a horizontal ADCP can provide a much longer time series of velocity profile, although there is only a single profile. This profile can nevertheless provide information of the velocity and velocity shear. In Li et al. (2018), horizontal ADCPs were used at three inlets of Barataria Bay including Barataria Pass (Fig. 5) with Sontek Argonaut ADCPs, all setup with 20-m bins and a total of 5 bins. The analysis was done to the averaged velocity of the 5 bins. The velocity shear was not examined in Li et al. (2018). As an example of showing the magnitude of velocity difference along the 160 m line, Fig. 6c shows the comparison of velocity time series between the east and west ends of the line. Obviously, the flow is not laterally uniform, as mentioned in (Li et al., 2011a; Cui et al., 2018).

The low pass filtered velocity components at 80 m away from the ADCP are shown in Fig. 6d. What is important here is that almost every peak for the low pass filtered velocity components corresponds to the timing of the passage of an atmospheric front, as already being shown by several recent studies. What has not been examined so far, however, is the velocity shear in response to the frontal events. With the velocity shear, we can estimate the relative vorticity pro-

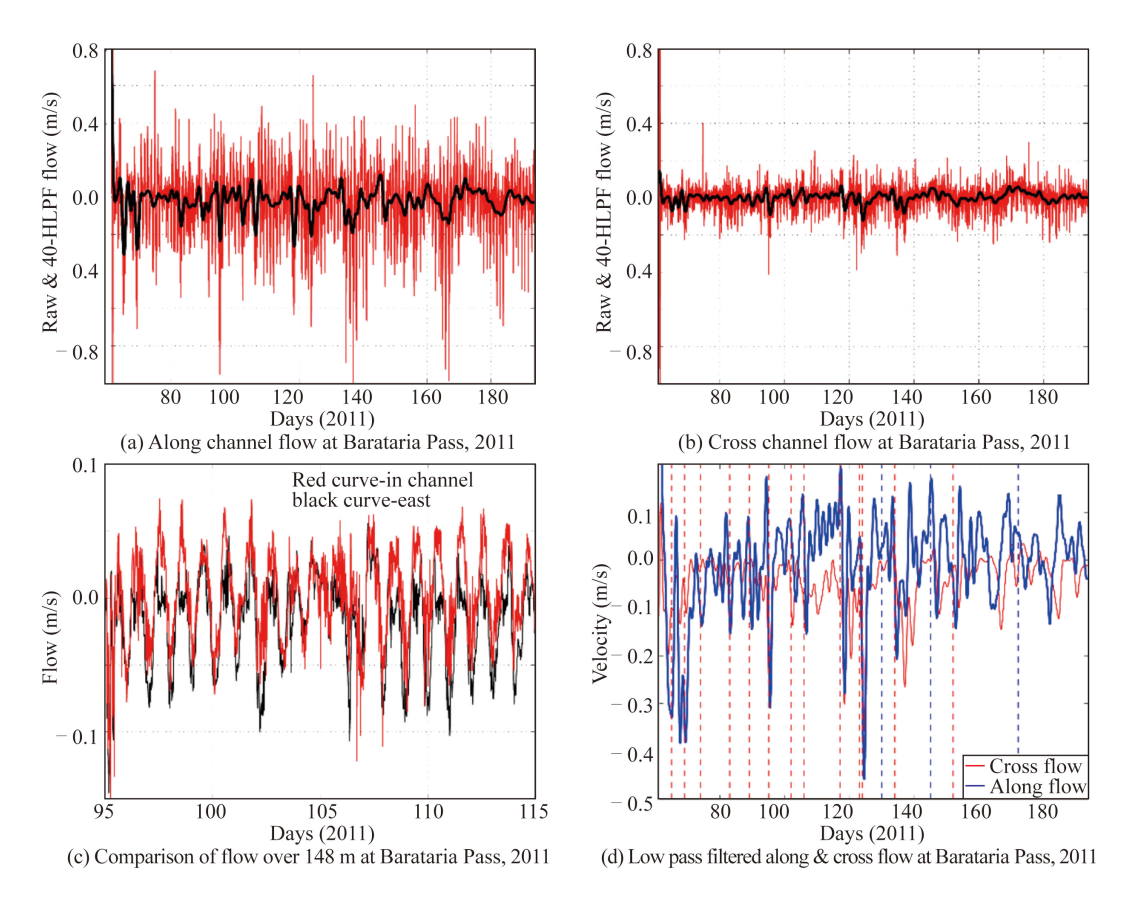
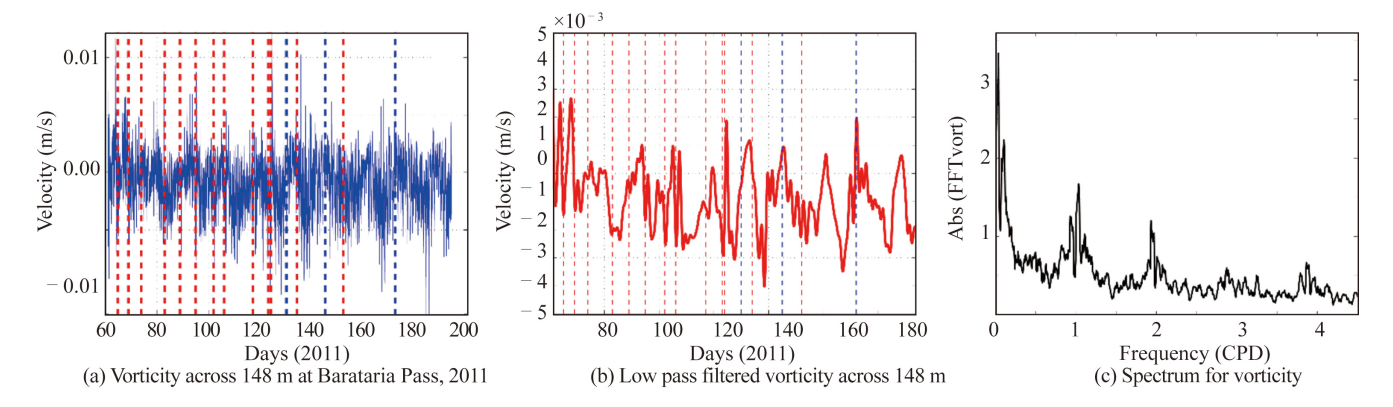


Fig. 6. Sample velocity data (a) the along channel flow (red line) and the 40-hour low pass filtered version (thick black line); (b) same as (a) but for the cross channel component; (c) comparison across the channel over 148 m for a selected period of time – the black curve is along channel velocity at the east end (bin 1, close to the shore), while the red curve is along channel velocity measured at bin 38, or  $\sim$  148 m further away from the east end where the black curve is measured; (d) compare the 40-hour low pass filtered velocity components at the far end of the transect in the along channel and cross channel directions for a selected period of time. The dashed vertical lines are the times of the atmospheric frontal passages.



**Fig. 7.** Relative vorticity. (a) Vorticity calculated from the lateral shear of the along channel velocity; vertical red dashed lines indicate timing of cold front; blue lines indicate other severe weather times such as during a stationary front with thunderstorm; (b) same as (a) but for low pass filtered vorticity; (c) spectrum of the vorticity, frequency is in cycle per day (CPD).

duced by the cross-channel variations of the along channel velocity (Fig. 7a).

The low pass filtered version of the vorticity is shown in Fig. 7b. Again, it is clear that the peaks and troughs of vorticity are consistent with the timings of frontal passages. This is significant because velocity shear and vorticity contribute to the dispersion, mixing, eddy generations, and turbulence (Fischer et al., 1979). The magnitude of this relative vorticity is on the order of  $\sim 10^{-3}$  s<sup>-1</sup> for the most part, but can reach  $\sim 10^{-2}$  s<sup>-1</sup> at times. The low pass filtered vorticity is also on the order of  $\sim 10^{-3}$  s<sup>-1</sup>. Compared to the planetary vorticity, which is  $\sim 10^{-4}$  s<sup>-1</sup>, these relative vorticity values are at least one order of magnitude larger and therefore the Earth's rotation effect is small, at least at the inlet.

We know that estuarine circulations at tidal frequencies can be affected by Earth's rotation (Pritchard, 1952; Kasai et al., 2000; Valle-Levinson et al., 2003; Sanay and Valle-Levinson, 2005), or planetary vorticity. At tidal frequencies, it was shown before (e.g. Li, 2002) that the relative vorticity can be 1–2 orders of magnitude higher than the planet-

ary vorticity at a narrow tidal inlet. Here the low pass filtered relative vorticity is also shown to be larger than the planetary vorticity at Barataria Pass under atmospheric frontal forcing.

The spectrum of vorticity (Fig. 7c) shows stronger diurnal and weaker semi-diurnal components. There are also smaller but obvious higher frequencies around 3 CPD and 4 CPD, which indicates nonlinear effects and shallow water constituents, typical in an inlet with nonlinearity. Most importantly, the low frequency part of the spectrum has a significant peak, indicating that the effect of weather is more important than tidal variations. In other words, the meteorological tide has more energy in this micro-tidal system.

To visualize the lateral variation of the spectra for the velocity components, the spectra for each bin at 4 m intervals are stacked together in Figs. 8 and 9. It can be seen that the lateral variation of spectrum does not appear to be obvious but some minor lateral variations do exist. It appears that flows have slightly stronger tidal signal at the eastern end of the transect near the ADCP and also at the far end of

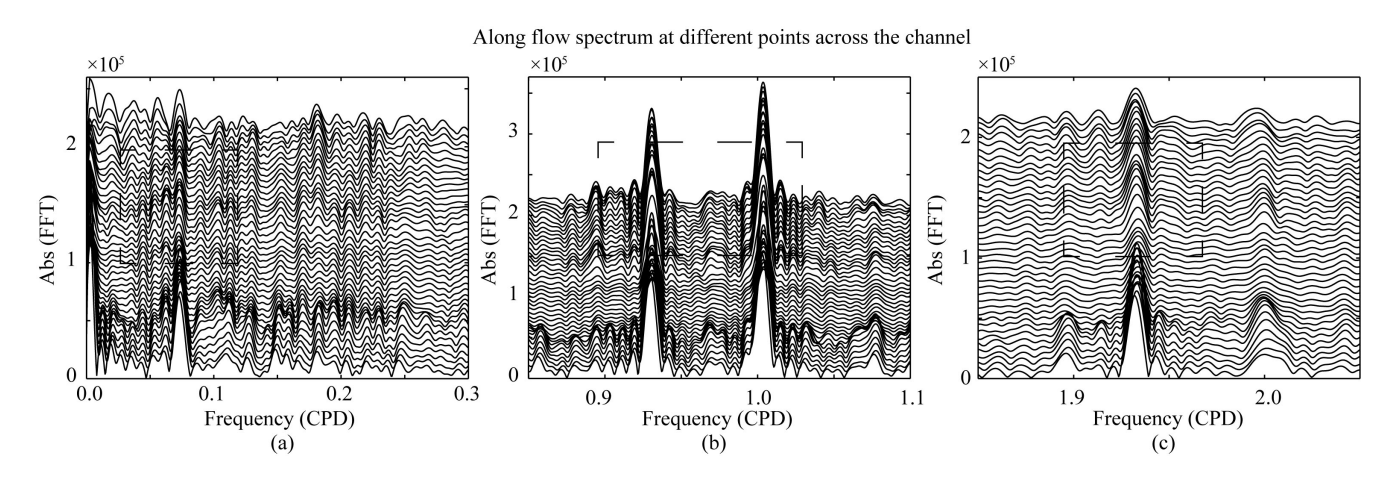


**Fig. 8.** Stacked plots of spectra for along channel velocity at various bins (positions) along the transect from the east end (lower lines) to 148 meters away at 4 m intervals. (a), (b), and (c) are zoomed-in for different frequency ranges, frequency is in cycle per day (CPD). The rectangles indicate the region with less dense stacked spectrum lines at tidal frequencies.

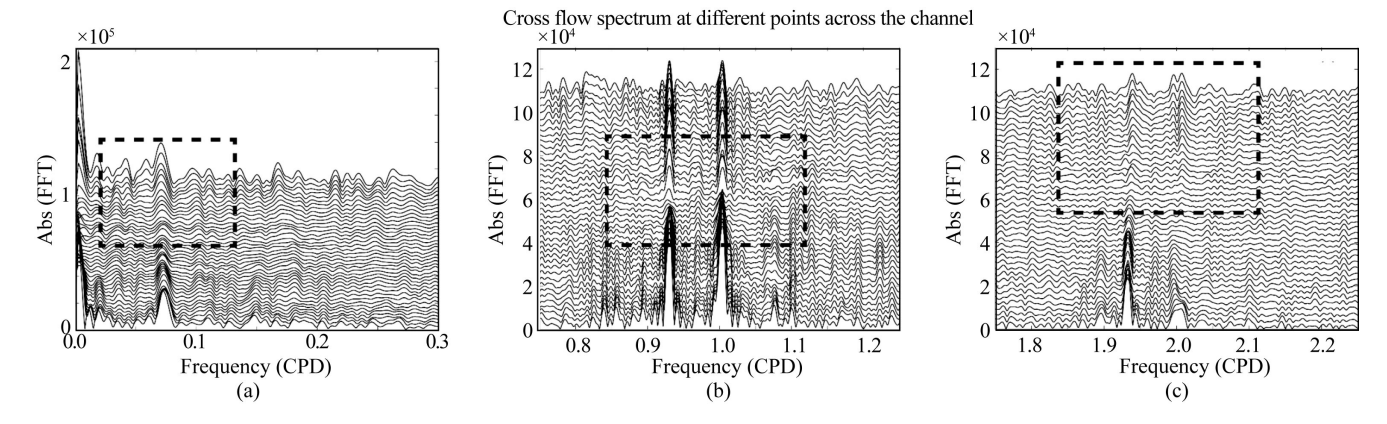


Fig. 9. Stacked plots of spectra for the cross-channel velocity at various bins (positions) along the transect from the east end (lower lines) to 148 meters away at 4 m intervals. (a), (b), and (c) are zoomed-in for different frequency ranges, frequency is in cycle per day (CPD). The rectangles indicate the region with less dense stacked spectrum lines at tidal frequencies.

the transect (at  $\sim$ 160 m from the ADCP). This is indicated by the less dense lines of the stacked spectra in the middle of the plot highlighted by the rectangles. The semi-diurnal tidal currents appear to have a redshift (the relevant spectrum line is slightly shifted toward the lower frequency end) at the western end of the transect (Fig. 9c). The reason of this slight shift is unknown but is probably insignificant to the overall dynamics, especially considering the fact that the meteorological tides have lower frequencies which are not affected by astronomical tides.

The mean velocity components as functions of the cross-channel distance are shown in Fig. 10. It is apparent that there is a consistent net outward flow along the transect. This net outward flow, however, has a significant lateral structure, so that the eastern end (in shallow water along the bank) has stronger outward flow, while the western half of the transect which is closer to the central channel (in deeper water) has much less outward flow. This is consistent with the model results of Wong (1994) for the estuarine circulation across an estuary with lateral depth variations (Fig. 1) in which the shallow shoals tend to have outward flows

while deep channels have inward flows. It is also consistent with earlier finding in Barataria Pass from vessel-based AD-CP measurements (Li et al., 2011a).

#### 4 Discussion

## 4.1 Scaling analysis and quasi-steady state balance

Now we do a quick order of magnitude estimate of the momentum equations based on the characteristics of the meteorological tides. It is a short version scaling analysis of Li et al. (2019a, 2019b) but using scales relevant to the data from this study. The two-dimensional momentum and continuity equations are

$$\frac{\partial u}{\partial t} + u \frac{\partial u}{\partial x} + v \frac{\partial u}{\partial y} - fv = -g \frac{\partial \zeta}{\partial x} + \frac{\tau_{ax}}{\rho(h+\zeta)} - \frac{\tau_{bx}}{\rho(h+\zeta)} - \frac{1}{\rho} \frac{\partial p_a}{\partial x};$$
(1)

$$\frac{\partial v}{\partial t} + u \frac{\partial v}{\partial x} + v \frac{\partial v}{\partial y} + fu = -g \frac{\partial \zeta}{\partial y} + \frac{\tau_{ay}}{\rho(h+\zeta)} - \frac{\tau_{by}}{\rho(h+\zeta)} - \frac{1}{\rho} \frac{\partial p_a}{\partial y};$$
(2

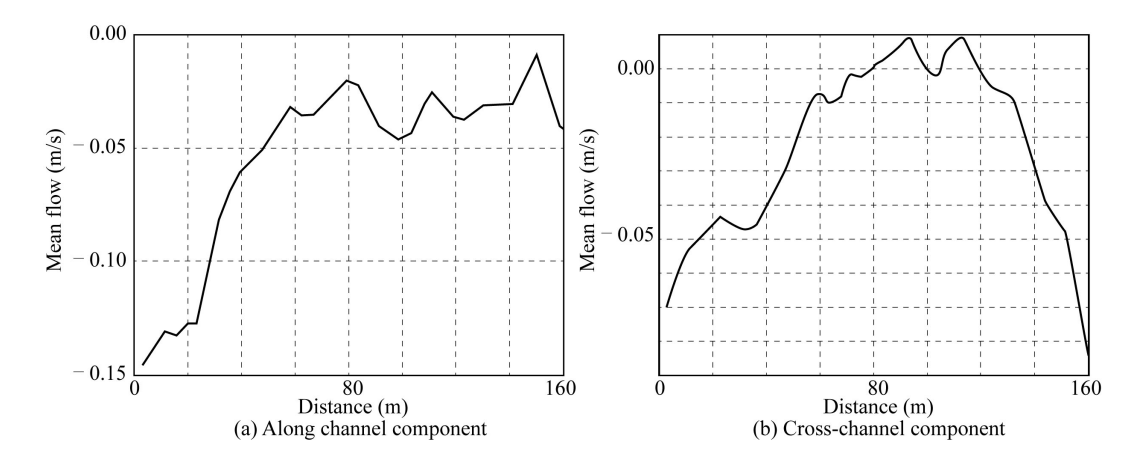


**Fig. 10.** Mean velocity distribution along the transect: (a) the along channel component; and (b) the cross-channel component of the temporal mean velocity. The *x*-axis is distance measured from the ADCP toward the southwest along the average beam of the transducers.

$$\frac{\partial \zeta}{\partial t} + \frac{\partial (h+\zeta)u}{\partial x} + \frac{\partial (h+\zeta)v}{\partial y} = 0,$$
(3)

in which  $u, v, \zeta, f, g, h, x, y, t, \rho, \tau_{ax}, \tau_{ay}, \tau_{bx}$ ,  $\tau_{by}$  and  $p_a$  are the depth-averaged east and north velocity components, surface elevation, Coriolis parameter, gravitational acceleration, depth, east and north coordinates, time, water density, east and north wind stress components, east and north bottom stress components, and sea-level atmospheric pressure, respectively. Each of the variables in the above equations should have a "high" frequency component (tidal or higher frequency oscillations) and a "low" frequency or "subtidal" component. For that reason, we can express the variables in terms of the superposition of the high and low frequency components:

$$u = u_H + u_L, v = v_H + v_L, \zeta = \zeta_H + \zeta_L.$$
 (4)

The subscripts H and L denote the high and low frequencies, respectively. The use of this expression is made with an implied assumption that the two frequency regimes (the high and low frequencies) represented in the above equations are "far apart". In other words, they can be effectively filtered out by a digital filter. As our interest is often the long-term effect, we can apply a low pass filter to keep only the low-frequency or the so called subtidal component (e.g.  $u_L$ ,  $v_L$ ,  $\zeta_L$ ), which is also the "meteorological tidal" component. Note that separating the high and low frequency components is not a problem because the meteorological tides cover mostly 0.1–0.3 CPD (Li et al., 2019a), while the high frequency component covers ~ 1 CPD and higher frequencies. It can be argued that for the first order approximation, the nonlinear terms are smaller. The linearized equations for the meteorological tidal motion are then:

$$\frac{\partial u_L}{\partial t} - f v_L = -g \frac{\partial \zeta_L}{\partial x} + \frac{\tau_{aLx}}{\rho h} - \frac{\tau_{bLx}}{\rho h} - \frac{1}{\rho} \frac{\partial p_{aL}}{\partial x}; \tag{5}$$

$$\frac{\partial v_L}{\partial t} + f u_L = -g \frac{\partial \zeta}{\partial y} + \frac{\tau_{aLy}}{\rho h} - \frac{\tau_{bLy}}{\rho h} - \frac{1}{\rho} \frac{\partial p_{aL}}{\partial y}; \tag{6}$$

$$\frac{\partial \zeta_L}{\partial t} + \frac{\partial h u_L}{\partial x} + \frac{\partial h v_L}{\partial y} = 0. \tag{7}$$

Since our data show that the variation in  $u_L$ ,  $v_L$  is  $\sim 0.5$  m/s over  $\sim 3$  days, while the change in  $\zeta_L$  is  $\sim 0.15$  m over 3 days. Consider that the bays have a spatial scale of  $\sim 10$  km and the channel has a width of smaller than 1 km, we can estimate that  $\frac{\partial u_L}{\partial t}$  and  $\frac{\partial v_L}{\partial t}$  are  $\sim 1.9 \times 10^{-6}$  m/s²,  $g \frac{\partial \zeta_L}{\partial x} \sim 1.5 \times 10^{-4} - 1.5 \times 10^{-3}$  m/s². This tells us that the local rate of change of the subtidal flow components are two to three orders of magnitude smaller than the subtidal pressure gradient force terms. Therefore, we can use the following approximate momentum equations:

$$-fv_L = -g\frac{\partial \zeta_L}{\partial x} + \frac{\tau_{aLx}}{\rho h} - \frac{\tau_{bLx}}{\rho h} - \frac{1}{\rho}\frac{\partial p_{aL}}{\partial x};$$
(8)

$$fu_L = -g\frac{\partial \zeta}{\partial y} + \frac{\tau_{aLy}}{\rho h} - \frac{\tau_{bLy}}{\rho h} - \frac{1}{\rho} \frac{\partial p_{aL}}{\partial y}.$$
 (9)

The wind stress is

$$\tau_{\mathbf{a}} = \rho_{\mathbf{a}} C_{\mathbf{D} \mathbf{a}} \mathbf{W} |\mathbf{W}|,\tag{10}$$

in which  $\tau_a$  is the wind stress vector,  $C_{Da}$  is the wind drag coefficient on the ocean surface, W is the wind velocity vector,  $\rho_a$  is the air density.

From this discussion, we can see that the meteorological tides satisfy a quasi-steady state momentum balance: although wind stress is changing with time, the momentum balance appears as a steady state at any instance. This conclusion is similar to those for Lake Pontchartrain (Huang and Li, 2017; Li et al., 2018) and confirms that inside the Barataria Bay (Li et al., 2019a), as well as in an arctic lagoon (Li et al., 2019a).

## 4.2 Meteorological tidal excursion

Tidal excursion is a range of distance a water particle can move within a tidal cycle. For example, under a diurnal tidal condition, if the average flood tidal current has an order of magnitude of  $\sim \bar{u}$ =0.5 m/s, the distance a particle can move during flood tide would be  $\bar{u} \times 12 \times \frac{3600}{1000} = 21.6$  km. During ebb tide, the particle would move backward for the same distance to where it started in the beginning of the flood tide. As a result, the tidal excursion in this case would be 21.6 km. As a rough estimate, it provides useful information on how far a water particle moves around due to tidal motion alone. Of course, nonlinear effects would induce a non-zero net excursion which however is generally smaller than the tidal excursion.

Likewise, we can estimate the particle excursion during a typical meteorological tidal event. If the average subtidal current during a cold front event has an order of magnitude of  $\sim \bar{u}=0.3$  m/s, and the time of inward flow is 1.5 days, the distance a particle can move during the "flood phase" of the meteorological tides would be  $\bar{u} \times 36 \times \frac{3600}{1000} \sim 38.9 \text{ km}.$ This is larger than the tidal excursion. The larger meteorological tidal excursion makes it much more likely that the estuarine particles get swept out of the estuary. In addition, meteorological tides are not periodic like the astronomical tide and the inward and outward flows are largely different and thus do not cancel with each other. This would result in a significant non-zero net flow. All these would make the particles less likely to return in the next cycle back into the estuary or end up at much different positions inside the estuary, leading to a more effective dispersion and transport of waterborne materials by the meteorological tides.

## 4.3 Air pressure effect to water level measurements

This subsection discusses only a technical issue of the correction of air pressure effect when the water level variations by the meteorological tides are measured using an underwater pressure sensor. This part of the discussion has

nothing to do with the dynamics of the meteorological tides. It however is important for data processing for the meteorological tides.

In a micro-tidal region, water level variations due to tides are relatively small. In contrast, the meteorological tidal effects are larger than tidally-induced flows (Li, 2013). With or without the presence of a severe weather event, the air pressure changes all the time, although the change is usually more significant during severe weather (Fig. 11). The water level measured from an underwater pressure sensor is the total pressure from both the water and air. The air pressure effect is sometimes corrected with a mean sea level air pressure (~1013 mb) but not with the observed air pressure. The resultant water level not corrected with the observed air pressure will have an error which is relatively large in a micro-tidal region. The conversion from pressure to water depth can be done with the following:

$$1 \text{ decibar (pressure)} = 1.01972 \text{ m (water depth)}$$
 (11)

Fig. 11 shows some examples of time series of the air pressure and water level from the study site. Again, the relatively large variations in the low pass filtered water level match in timings of the frontal passages quite well. Fig. 12 compares the water level corrected by using the observed

sea-level air pressure and that corrected with a mean pressure of 1013 mb. The difference can be quite significant ( $\pm 0.2$  m). The range is 0.4 m which is 2/3 of the maximum tidal range. This is better visualized and quantified by Fig. 13 which shows the sea level air pressure from Grand Isle near our ADCP site and the water level correction resulted from the air pressure change. The correction is on the order of  $\pm 0.2$  m. The maximum values all occur during atmospheric frontal passages when the air pressure first drops to its minimum when a front passes and then increases to its maximum after the frontal passage.

#### 4.4 Predictability of meteorological tides

Astronomical tides can be predicted given enough historic data for a statistical regression. It might appear to be difficult for the meteorological tides to be predictable as they do not have a well-defined line spectrum. Instead, the "oscillation" is rather irregular and the spectrum is continuous so that a harmonic analysis similar to that for tides wouldn't be appropriate. Another reason for the challenge is that weather cannot be reliably predicted beyond a short ~ 10-day window whereas tidal predictions can be done many years ahead. However, recent studies have shown that, giv-

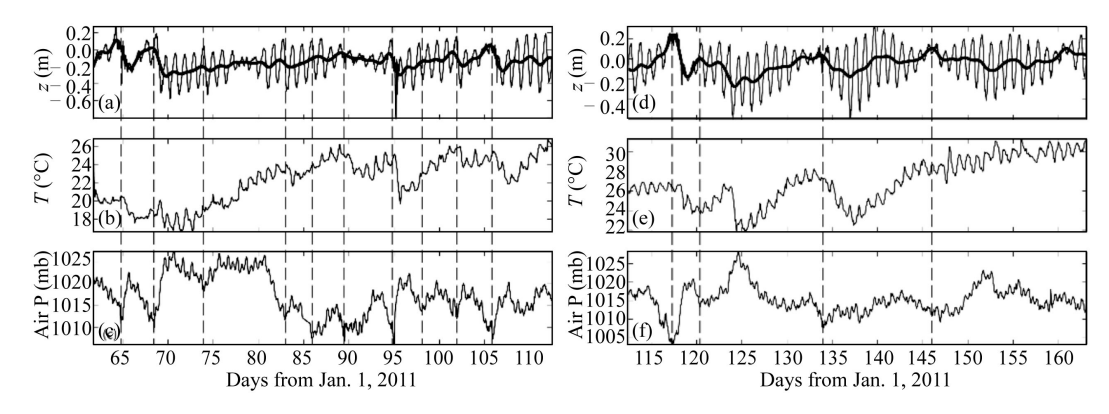


Fig. 11. Examples of time series of water level (along with its low pass filtered curve), water temperature, and sea level air pressure at the study site. The vertical dashed lines indicate the timing of cold fronts.

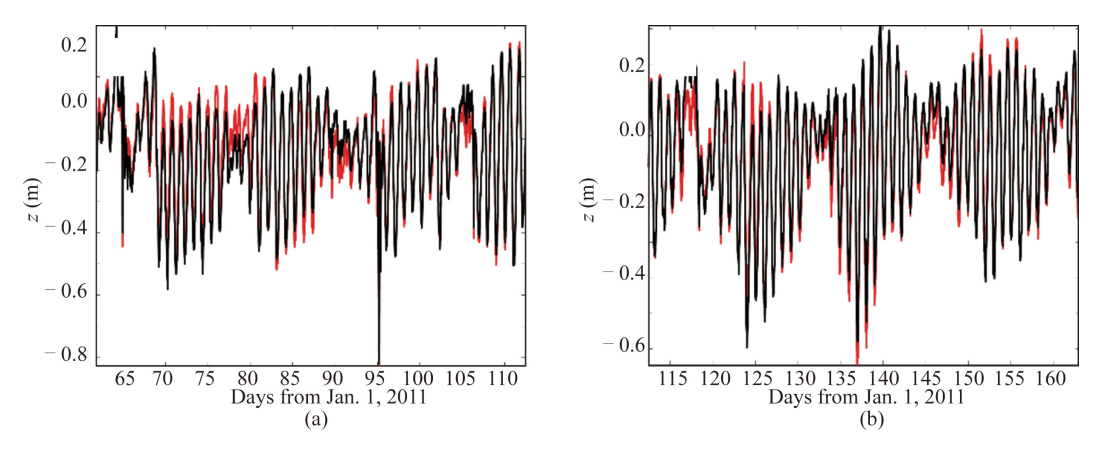
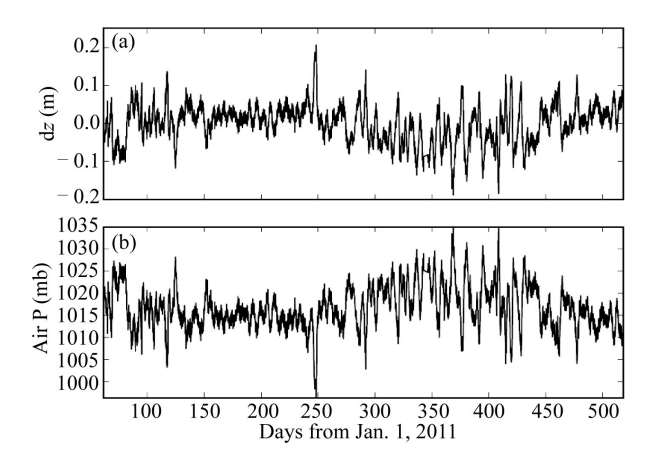


Fig. 12. Examples of water level from the pressure sensor on the ADCP corrected using a mean sea level air pressure (1013 mb) (red lines) and that corrected with actual observed sea level air pressure (black lines).



**Fig. 13.** Example of (a) time series of correction to water level data based on the sea-level air pressure, and (b) time series of the sea-level air pressure.

en wind stress, the meteorological tidal currents can be reliably calculated at locations with sufficient historic data, using a regression model based on a Taylor series expansion (Li et al., 2019a, 2019b). This regression model is also based on the quasi-steady state discussed earlier. More specifically, the along channel velocity at an inlet is given by the following model:

$$u(t) = AW_x(t) + BW_x^2(t) + CW_y(t) + DW_y^2(t) + E(p - \bar{p}) + F$$
(12)

in which u(t),  $W_x(t)$ ,  $W_y(t)$ , p, and  $\bar{p}$  are, respectively, the time series of the low pass filtered along channel velocity component, the east wind velocity component, the north wind velocity component, the air pressure, and the mean air pressure (averaged over time); t is time; A, B, C, D, E, and F are regression coefficients. The east and north wind components can be replaced by the along channel and cross channel wind velocity components as done in Li et al. (2019a). In these calculations, all variables are 40-hr low pass filtered by a Butterworth Infinite Impulse Response filter (Butterworth, 1930; Emery and Thomson, 2001). The reason to use this filter with a 40-hour cutoff is because this region is dominated by diurnal tides therefore a 40-hour cutoff period would take out the tidal oscillations. In addition, this filter has an advantage of close to 100% energy recovery below the cutoff frequency (Li et al., 2011b, 2019a). It has a relatively narrow and monotonic transition band, and an almost 100% cutoff beyond the cutoff frequency. This filter is known as the "maximum flat magnitude" filter because it can quite accurately preserve the pass band energy (Li et al., 2011b). Fig. 14 is drawn using the regression coefficients from Li et al. (2019a) in which the regression model calculated velocity is compared with data obtained at Barataria Pass in 2014.

Obviously, the regression model results match the observational data quite well. The  $R^2$  value is between 0.48 and 0.58 in the three major inlets of Barataria Bay (Li et al.,

2019a). The regression model was also applied to an arctic tidal inlet of the northernmost lagoon of the U.S.-the Elson Lagoon-with much higher  $R^2$  values of up to 0.96 (Li et al., 2019b). In a recent study of atmospheric front induced exchange flows in the Calcasieu Lake Estuary, this regression model was applied and the comparison with data had an  $R^2$  value of about 0.7.

The reason for the relatively lower  $R^2$  values for the Barataria Bay is most likely due to the fact that the estuary has complicated multiple inlets and is surrounded by wetland. In very shallow waters, nonlinear effect would be large which may introduce more complexity than the regression model can capture. The fact that the regression in the Calcasieu Lake Estuary has a higher  $R^2$  value than those of Barataria Bay is reasonable because Calcasieu Lake has only a single elongated inlet. It however is surrounded by wetland as well. The wetland is connected to the estuary through some water control structures (Hoese and Konikoff, 1995; Kimball et al., 2015; Lin et al., 2016) and the exchange is thus limited.

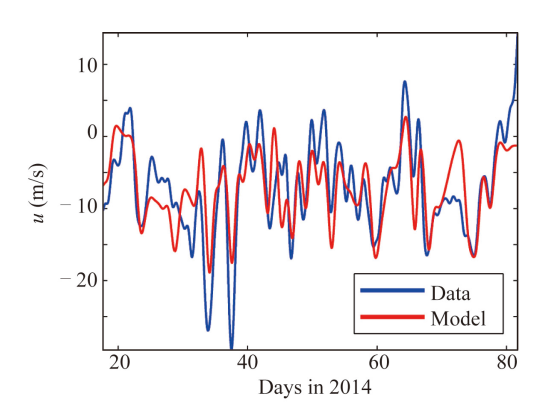


**Fig. 14.** Comparison between low pass filtered observed velocity and regression model calculated velocity (using the regression coefficients and data from Li et al., 2019a).

## 4.5 Implications to future research

There have been many studies on weather- or wind-induced motions in the coastal ocean and estuaries. However, when we consider the problem in a framework of meteorological tides, we recognize the repetitive nature of the weather events and the effects of long-term integration. That is what makes the study of meteorological tides different from a study of an isolated wind-driven motion. In that sense, the study of meteorological tides is from a holistic point of view and is still not well established yet in terms of the global coverage. The recent studies including that presented here have shown a need and direction for continued research on meteorological tides. Unlike astronomical tides, meteorological tides are much less regular and therefore the factors that control weather and climate will play roles in determining the effects of the meteorological tides. For that reason, there must be regional differences, given other factors identical. Of cause, even aside from meteorological forcing, "other factors" can never be really "identical": bays and estuaries are all unique in their shapes and connections to their environment. Complications do not stop here — the climate change may alter the frequencies and intensities of meteorological tides as we have seen from Fig. 4: the upward trend of the number of atmospheric frontal events over 40 years. This brings up several other issues. One of them is the meteorological tide induced erosion, sediment transport and the geomorphological effects may all change with time with the increasing number of weather events. In this context, the integrated effect is of most interest. In general, the short-term (e.g. seasonal) and long-term ecological impacts of meteorological tides are also of great interest and can be subjects of studies.

#### 5 Conclusions

Meteorological tides are quasi-periodic with continuous spectra. This is contrary to the astronomical tides which have discrete (or line) spectra. Meteorological tides depend on the synoptic scale atmospheric systems. Such a weather system usually occupies a few thousands of kilometers at any one instance. The atmospheric systems include cold and warm fronts and associated extratropical cyclones that occur once every few days in the northern Gulf of Mexico region (and many other places around the world). Because of these reasons, it is important to recognize the importance of these recurring processes in driving estuarine circulations. The traditional studies are often biased toward the fairweather end-members due to difficulties in conducting vessel-based surveys during rough conditions. The present study further extends the time period to 40 years for the contiguous U.S. to consider the number of frontal events every year and an additional case study was conducted. This study allowed us to conclude that -

- (1) Within the record of 40 years of weather for the contiguous U.S. between Jan. 1, 1977 and Dec. 31, 2016 there were a total of 1648 frontal events, averaging  $41.2\pm4.7$  per year.
- (2) It is found that January has the maximum number of 40-year averaged frontal events  $\sim 6.3$  fronts per month. December has a smaller number ( $\sim 5.8/\text{month}$ ), followed by February with 5.7/month. November and March have the same average numbers (5.55/month), while October ( $\sim 4.5/\text{month}$ ) and April ( $\sim 4.8/\text{month}$ ) are lower and September ( $\sim 3/\text{month}$ ) has the minimum.
- (3) There is an upward trend of the number of frontal events over the 40-year period. The rate of increase is about 0.2039 per year, leading to an increase of  $\sim 8.15$  fronts per year at the end of the 40 years (2016 compared to 1977).
- (4) These frontal events are what drive the meteorological tides. The observations at Barataria Pass in 2011 corroborate with the results using data from 2014–2015 that meteorological events influence the low pass filtered (sub-

- tidal) flows significantly (Li et. al., 2019b).
- (5) In addition, the 2011 data discussed here allowed the examination of velocity shears and relative vorticity. It is found that the relative vorticity is much stronger than the planetary vorticity at the study site. Like the low pass filtered flows, the low pass filtered vorticity also shows significant response to the weather events. The associated dispersion and mixing must also increase quasi-periodically under meteorological tides.
- (6) The scaling analysis indicates that the dynamical process of meteorological tides is quasi-steady state, i.e. the local acceleration or local rate of change of the velocity is negligible compared to pressure gradient and stress terms in the momentum equations.
- (7) The particle excursions under meteorological tides are larger than the tidal excursion. Because of the irregular nature, the inward and outward flows do not cancel with each other and the particles have much greater chance to move out of the estuaries and not return in the next cycle, which can be a mechanism for greater and more efficient water and material dispersion and exchange.
- (8) The regression model is a useful tool for prediction of the meteorological tidal currents because it only depends on the prediction of wind velocity which is nowadays reliable for  $\sim 5-7$  days, given that some data of flow are available for calculating the regression coefficients. In addition to the predictions, hindcast can also be done for the meteorological tide induced exchange flows for a long period of time as demonstrated in Li et al. (2019b) and Wang et al. (2020).

## References

Aubrey, D.G. and Friedrichs, C.T., 1996. Buoyancy Effects on Coastal and Estuarine Dynamics, American Geophysical Union, American, pp. 99359.

Barlow, J.P., 1956. Effect of wind on salinity distribution in an estuary, *Journal of Marine Research*, 15, 193–203.

Butterworth, S., 1930. On the Theory of filter amplifiers, *Experimental Wireless and the Wireless Engineer*, 7, 536–541.

Chant, R.J. and Wilson, R.E., 1997. Secondary circulation in a highly stratified estuary, *Journal of Geophysical Research: Oceans*, 102(C10), 23207–23215.

Charlton, J.A., McNicoll, W. and West, J.R., 1975. Tidal and freshwater induced circulation in the Tay Estuary, *Proceedings of the Royal Society of Edinburgh*, *Section B: Biological Sciences*, 75(1–2), 11–27

Chuang, W.S. and Swenson, E.M., 1981. Subtidal water level variations in Lake Pontchartrain, Louisiana, *Journal of Geophysical Research: Oceans*, 86(C5), 4198–4204.

Chuang, W.S. and Wiseman Jr., W.J., 1983. Coastal sea level response to frontal passages on the Louisiana-Texas Shelf, *Journal of Geophysical Research: Oceans*, 88(C4), 2615–2620.

Cui, L.L., Huang, H.S., Li, C.Y. and Justic, D., 2018. Lateral circulation in a partially stratified tidal inlet, *Journal of Marine Science and Engineering*, 6(4), 159.

de Miranda, L.B., Andutta, F.P., Kjerfve, B. and de Castro Filho, B.M., 2017. Fundamentals of Estuarine Physical Oceanography,

- Springer, Singapore, pp. 480.
- Doyle, B.E. and Wilson, R.E., 1978. Lateral dynamic balance in the Sandy Hook to Rockaway Point transect, *Estuarine and Coastal Marine Science*, 6(2), 165–174.
- Elliott, A.J., 1978. Observations of the meteorologically induced circulation in the Potomac Estuary, *Estuarine and Coastal Marine Science*, 6(3), 285–299.
- Emery, W.J. and Thomson, R.E., 2001. *Data Analysis Methods in Physical Oceanography*, second ed., Elsevier, Amsterdam.
- Fang, G.H. and Yang, J.F., 1985. A two-dimensional numerical model of the tidal motions in the Bohai Sea, *Chinese Journal of Oceano*logy and *Limnology*, 3(2), 135–152.
- Feng, Z.X. and Li, C.Y., 2010. Cold-front-induced flushing of the Louisiana Bays, *Journal of Marine Systems*, 82(4), 252–264.
- Fischer, H.B., List, J.E., Koh, R.C.Y., Imberger, J. and Brooks, N.H., 1979. Mixing in Inland and Coastal Waters, Academic Press, New York, pp. 483.
- Forbes Jr., M.J., 1988. *Hydrologic Investigations of the Lower Calcasieu River, Louisiana*, Louisiana Department of Environmental Quality Office of Water Resources, Baton Rouge.
- Friedrichs, C.T. and Aubrey, D.G., 1994. Tidal propagation in strongly convergent channels, *Journal of Geophysical Research: Oceans*, 99(C2), 3321–3336.
- Geyer, R.W., 1993. Three-dimensional tidal flow around headlands, *Journal of Geophysical Research: Oceans*, 98(C1), 955–966.
- Hansen, D.V. and Rattray Jr., M., 1965. Gravitational circulation in straits and estuaries, *Journal of Marine Research*, 23(1), 104–122.
- Harris, D.L., 1981. *Tides and Tidal Datums in the United States*, U.S. Army Engineer Waterways Experiment Station, Vicksburg, pp. 382.
- Herrling, G. and Winter, C., 2015. Tidally- and wind-driven residual circulation at the multiple-inlet system East Frisian Wadden Sea, *Continental Shelf Research*, 106, 45–59.
- Hoese, H.D. and Konikoff, M., 1995. Effects of marsh management on fisheries organisms: The compensatory adjustment hypothesis, *Estu-aries*, 18(1), 180–197.
- Holton, J.R. and Hakim, G.J., 2012. An Introduction to Dynamic Meteorology, fifth ed., Elsevier, New York, pp. 524.
- Huang, W. and Li, C.Y., 2017. Cold front driven flows through multiple inlets of Lake Pontchartrain Estuary, *Journal of Geophysical Research: Oceans*, 122(11), 8627–8645.
- Huang, W. and Li, C.Y., 2019. Spatial variation of cold front winddriven circulation and quasi-steady state balance in Lake Pontchartrain Estuary, *Estuarine*, *Coastal and Shelf Science*, 224, 154–170.
- Ianniello, J.P., 1977. Tidally induced residual currents in estuaries of variable breadth and depth, *Journal of Marine Research*, 35, 755-785.
- Ianniello, J.P., 1979. Tidally induced residual currents in estuaries of variable breadth and depth, *Journal of Physical Oceanography*, 9(5), 962–974.
- Kasai, A., Hill, A.E., Fujiwara, T. and Simpson, J.H., 2000. Effect of the Earth's rotation on the circulation in regions of freshwater influence, *Journal of Geophysical Research*: *Oceans*, 105(C7), 16961–16969.
- Keen, T.R. and Stavn, R.H., 2012. Hydrodynamics and marine optics during cold fronts at Santa Rosa Island, Florida, *Journal of Coastal Research*, 28(5), 1073–1087.
- Kimball, M.E., Rozas, L.P., Boswell, K.M. and Cowan Jr., J.H., 2015. Effects of slotted water control structures on nekton movement within salt marshes, *Marine and Coastal Fisheries: Dynamics, Man-*

- agement, and Ecosystem Science, 7(1), 177-189.
- Kineke, G.C., Higgins, E.E., Hart, K. and Velasco, D., 2006. Fine-sediment transport associated with cold-front passages on the shallow shelf, Gulf of Mexico, *Continental Shelf Research*, 26(17–18), 2073–2091.
- Kjerfve, B., 1973. *Dynamics of the Water Surface in a Bar-Built Estu*ary, Ph.D. Thesis, Louisiana State University, Baton Rouge, pp. 91.
- Li, C.Y. and Chen, C.S., 2014. Shelf circulation prior to and post a cold front event measured from vessel-based acoustic Doppler current profiler, *Journal of Marine Systems*, 139, 38–50.
- Li, C.Y. and O'Donnell, J., 1997. Tidally driven residual circulation in shallow estuaries with lateral depth variation, *Journal of Geophysical Research: Oceans*, 102(C13), 27915–27929.
- Li, C.Y. and O'Donnell, J., 2005. The effect of channel length on the residual circulation in tidally dominated channels, *Journal of Physical Oceanography*, 35(10), 1826–1840.
- Li, C.Y., 2002. Axial convergence fronts in a barotropic tidal inlet-sand shoal inlet, *VA*, *Continental Shelf Research*, 22(18–19), 2633–2653.
- Li, C.Y., 2013. Subtidal water flux through a multiple-inlet system: Observations before and during a cold front event and numerical experiments, *Journal of Geophysical Research*: *Oceans*, 118(4), 1877–1892.
- Li, C.Y., Boswell, K.M., Chaichitehrani, N., Huang, W. and Wu, R.H., 2019a. Weather induced subtidal flows through multiple inlets of an arctic microtidal lagoon, *Acta Oceanologica Sinica*, 38(3), 1–16.
- Li, C.Y., Chen, C.S., Guadagnoli, D. and Georgiou, I.Y., 2008. Geometry-induced residual eddies in estuaries with curved channels: Observations and modeling studies, *Journal of Geophysical Research: Oceans*, 113(C1), C01005.
- Li, C.Y., Huang, W. and Milan, B., 2019b. Atmospheric cold front-induced exchange flows through a Microtidal multi-inlet bay: Analysis using multiple horizontal ADCPs and FVCOM simulations, *Journal of Atmospheric and Oceanic Technology*, 36(3), 443–472.
- Li, C.Y., Roberts, H., Stone, G.W., Weeks, E. and Luo, Y.X., 2011b. Wind surge and saltwater intrusion in Atchafalaya Bay during onshore winds prior to cold front passage, *Hydrobiologia*, 658(1), 27–39.
- Li, C.Y., Valle-Levinson, A., Wong, K.C. and Lwiza, K.M.M., 1998. Separating baroclinic flow from tidally induced flow in estuaries, *Journal of Geophysical Research: Oceans*, 103(C5), 10405–10417.
- Li, C.Y., Weeks, E., Huang, W., Milan, B. and Wu, R.H., 2018. Weather-induced transport through a tidal channel calibrated by an unmanned boat, *Journal of Atmospheric and Oceanic Technology*, 35(2), 261–279.
- Li, C.Y., White, J.R., Chen, C.S., Lin, H.C., Weeks, E., Galvan, K. and Bargu, S., 2011a. Summertime tidal flushing of Barataria Bay: Transports of water and suspended sediments, *Journal of Geophysical Research*: *Oceans*, 116(4), C04009.
- Li, Y.D., Li, C.Y. and Li, X.F., 2017. Remote Sensing studies of suspended sediment concentration variations in a coastal bay during the passages of atmospheric cold fronts, *IEEE Journal of Selected Topics in Applied Earth Observations and Remote Sensing*, 10(6), 2608–2622.
- Lin, J., Li, C.Y., Boswell, K.M., Kimball, M. and Rozas, L., 2016. Examination of winter circulation in a northern gulf of Mexico estuary, *Estuaries and Coasts*, 39(4), 879–899.
- Maddock, L. and Pingree, R.D., 1978. Numerical simulation of the Portland tidal eddies, *Estuarine and Coastal Marine Science*, 6(4), 353–363.

- Moeller, C.C., Huh, O.K., Roberts, H.H., Gumley, L.E. and Menzel, W.P., 1993. Response of Louisiana coastal environments to a cold front passage, *Journal of Coastal Research*, 9(2), 434–447.
- Officer, C.B., 1976. Physical Oceanography of Estuaries (and Associated Coastal Waters), Wiley, New York, pp. 465.
- Pingree, R.D. and Maddock, L., 1977a. Tidal eddies and coastal discharge, *Journal of the Marine Biological Association of the United Kingdom*, 57(3), 869–875.
- Pingree, R.D. and Maddock, L., 1977b. Tidal residuals in the English Channel, *Journal of the Marine Biological Association of the United Kingdom*, 57(2), 339–354.
- Pingree, R.D. and Maddock, L., 1979. The tidal physics of headland flows and offshore tidal bank formation, *Marine Geology*, 32(3–4), 269–289
- Pingree, R.D., 1978. The formation of the shambles and other banks by tidal stirring of the seas, *Journal of the Marine Biological Association of the United Kingdom*, 58(1), 211–226.
- Prandle, D., 2009. Estuaries Dynamics, Mixing, Sedimentation and Morphology, Cambridge University Press, New York.
- Pritchard, D.W., 1952. Salinity distribution and circulation in the Chesapeake Bay estuarine system, *Journal of Marine Research*, 11, 106–123.
- Pritchard, D.W., 1954. A study of the salt balance in a coastal plain estuary, *Journal of Marine Research*, 13(1), 133–144.
- Pritchard, D.W., 1956. The dynamic structure of a coastal plain estuary, *Journal of Marine Research*, 15, 33–42.
- Roberts, H.H., DeLaune, R.D., White, J.R., Li, C.Y., Sasser, C.E., Braud, D., Weeks, E. and Khalil, S., 2015. Floods and cold front passages: impacts on coastal marshes in a river diversion setting (wax lake delta area, Louisiana), *Journal of Coastal Research*, 31(5), 1057–1068.
- Roberts, H.H., Huh, O.K., Hsu, S.A., Rouse Jr., L.J. and Rickman, D.A., 1989. Winter storm impacts on the Chenier plain coast of southwestern Louisiana, *Gulf Coast Association of Geological Societies Transactions*, 39, 515–522.
- Roberts, H.H., Huh, O.K., Hsu, S.A., Rouse, L.J. and Rickman, D., 1987. Impact of cold-front passages on geomorphic evolution and sediment dynamics of the complex Louisiana coast, In: *Proceedings* of Coastal Sediments '87, American Society of Civil Engineers,

- New Orleans, Louisiana, pp. 1950-1963.
- Robinson, A.H.W., 1960. Ebb-flood channel systems in sandy bays and estuaries, *Geography*, 45(3), 183–199.
- Sanay, R. and Valle-Levinson, A., 2005. Wind-induced circulation in Semienclosed homogeneous, rotating Basins, *Journal of Physical Oceanography*, 35(12), 2520–2531.
- Schoen, J.H., Stretch, D.D. and Tirok, K., 2014. Wind-driven circulation patterns in a shallow estuarine lake: St Lucia, South Africa, Estuarine, Coastal and Shelf Science, 146, 49–59.
- Siadatmousavi, S.M. and Jose, F., 2015. Winter storm-induced hydrodynamics and morphological response of a shallow transgressive shoal complex: Nnorthern Gulf of Mexico, *Estuarine*, *Coastal and Shelf Science*, 154, 58–68.
- Signell, R.P. and Geyer, W.R., 1991. Transient eddy formation around headlands, *Journal of Geophysical Research*: *Oceans*, 96(C2), 2561–2575.
- Stommel, H.M. and Farmer, H.G., 1952. On the nature of estuarine circulation, in: Woods Hole Oceanographic Institution Reference No.52-88. Part I (Chapters 3–4).
- Valle-Levinson, A., 2010. Contemporary Issues in Estuarine Physics, Cambridge University Press, New York, pp. 315.
- Valle-Levinson, A., Reyes, C. and Sanay, R., 2003. Effects of bathymetry. friction, and rotation on estuary-ocean exchange, *Journal of Physical Oceanography*, 33(11), 2375–2393.
- Wang, J., Li, C.Y., Xu, F.M. and Huang, W., 2020. Severe weather-induced exchange flows through a narrow tidal channel of Calcasieu Lake Estuary, *Journal of Marine Science and Engineering*, 8(2), 113
- Weeks, E., Robinson, M.E.and Li, C.Y., 2018. Quantifying cold front induced water transport of a bay with *in situ* observations using manned and unmanned boats, *Acta Oceanologica Sinica*, 37(11), 1–7
- Wolanski, E., Asaeda, T., Tanaka, A. and Deleersnijder. E., 1996. Three-dimensional island wakes in the field, laboratory experiments and numerical models, *Continental Shelf Research*, 16(11), 1437–1452.
- Wong, K.C., 1994. On the nature of transverse variability in a coastal plain estuary, *Journal of Geophysical Research: Oceans*, 99(C7), 14209–14222.